Shear lag effects on pedestrian-induced vibration and TMD-based vibration control of footbridges

Bo Fu[1], Xinxin Wei[2,*], Jin Chen[1], Sifeng Bi[3]

[1] School of Civil Engineering, Chang'an University, Xi'an 710061, China

[2] Ruhr-Universität Bochum, Universitätsstraße 150, D- 44780 Bochum, Germany

[3] School of Aerospace Engineering, Beijing Institute of Technology, No. 5, Zhongguancun South Street, Beijing 100081, China

[*] **Correspondence author:** Xinxin Wei, Ruhr-Universität Bochum, Universitätsstraße 150, D-44780 Bochum, Germany (**wei_xinxin@hotmail.com**)

Abstract

The Shear Lag Effect (SLE) is one of the vital mechanical characteristics of structures with thin-walled box section. While most of the existing studies on SLE focus on the static response of footbridges, the pedestrian-induced vibration deserves more attention since it represents the actual response of footbridges during their practical service process. The theoretical framework is proposed to consider the corresponding SLE. Firstly, the SLE on the natural frequencies of the structure can be considered with a reduction ratio to the corresponding case without considering SLE (the classic solutions of natural frequencies). Results show that, the footbridges with smaller span-width ratios, smaller section thickness-width ratios, and lower height-width ratios are more necessary to consider the SLE. Furthermore, although the Poisson's ratio effects are relatively lower than other aspects, the steel bridges still need to be paid to attention for the SLE. Due to the SLE, it may result in significant reductions in the natural frequencies of the structures. These reductions in the predicted natural frequencies due to the SLE may further result in inaccuracy in the prediction of pedestrian-induced vibrations of the footbridges. Furthermore, the most often applied mitigation measures may not be reliably designed. It may result in very significant reduction in the effectiveness of the vibration mitigation measures. To consider the SLE on pedestrian-induced vibration and TMD-based vibration control of typical footbridges with thin-walled box section, a simplified strategy is proposed.

This is a peer-reviewed, accepted author manuscript of the following article: Fu, B., Wei, X., Chen, J., & Bi, S. (2022). Shear lag effects on pedestrian-induced vibration and TMD-based vibration control of footbridges. Structural Engineering International. https://doi.org/10.1080/10168664.2022.2059799

Keywords: human-induced vibration; footbridges; vibration serviceability; shear lag effect; thin-walled box section; tuned mass damper

1. Introduction

Pedestrian-induced vibration of footbridges

A reliable prediction of pedestrian-induced structural responses is extremely crucial when designing slender footbridges [1-4] and other civil engineering structures with low natural frequencies and damping capacity [5-6]. According to current guidelines such as Sétra [7] and HiVoSS [8], vibration serviceability assessments of footbridges are based on comparisons between relevant comfort criteria and predicted vibration levels to the human excitation [9-14]. For existing studies of evaluating the pedestrian-induced footbridge vibration [15-17], it often considers the structure as an equivalent single degree of freedom (SDOF), of which its natural frequency falls into the frequency range of human excitations. This methodology works in most cases because pedestrian-induced structural responses of slender footbridges are often dominated by a single mode; whereas sometimes it needs to consider multi-mode contributions, e.g., when closely-spaced natural frequencies are found in real-world footbridges [18-20]. More importantly, to obtain reliable response predictions, it should be identified or pre-know as accurate as possible the natural frequencies of the structure [14], which are very important parameters in the governing equations of motion of the structure.

Vibration control of footbridges

To attenuate vibration levels of footbridges, various structural control methods are adopted. Among them, the passive tuned mass damper (TMD) is most widely applied due to its simplicity, low cost and effectiveness. For instance, Caetano et al. [21] experimentally studied the damping effect of the TMD on the Pedro e Inês footbridge in Portugal. To improve the performance of TMDs in controlling the pedestrian-induced vibrations on footbridges considering the uncertainties of their modal properties, Jiménez-Alonso and Sáez [22] conducted a robust optimum design by using multi-objective genetic algorithms. Qin et al. [23] installed a self-made TMD using lead, spring and oil buffer on a scaled single pylon cable-stayed footbridge model and investigated the effectiveness of the TMD by conducting laboratory forced vibration tests. To address the detuning issue of the passive TMD, some advanced structural control techniques were recently adopted by the researchers. Li et al. [24] used the multiple tuned mass dampers (MTMD) in suppressing the crowd-induced vibration and proposed a design method of MTMD via a random optimization procedure. Wang et al. [25] also compared the control effectiveness of the MTMD with the single TMD on long-span steel footbridges by performing site measurement and numerical simulation. They concluded that the MTMD has superior vibration adsorption robustness and stable capacity in reducing structural vibrations under crowd loads. Casado et al. [26] adopted an active mass damper (AMD) system in controlling crowd-induced vibrations of footbridges. They found that although the AMD is very effective and robust, there are still some disadvantages such as cost should be resolved. Moutinho et al. [27] applied a semiactive TMD including a magneto-rheological (MR) damper to reduce vibrations of a slender footbridge. The semiactive TMD is capable to perform multimodal control. Similarly, Contreras-Lopez et al. [28] proposed a nonlinear optimal semiactive control strategy for attenuating footbridge vibration using MR dampers. It is worthwhile to point out that, to determine the design parameters of the TMD, resonant conditions are assumed, i.e., resonance with the targeted mode where the TMD is tuned. Thus, except for the excitation frequency, effectiveness of TMD-based vibration control relies mainly on the accuracy of the natural frequency of the considered mode of the structure.

Studies on the Shear Lag Effect (SLE) and research gaps

The thin-walled box section, also known as hollow cross section, is widely used in footbridges because of its light weight and good mechanical properties. As for thin-walled box section, the Shear Lag Effect (SLE) is one of the vital mechanical characteristics and has been widely investigated, however, most of the studies on the SLE focus on static responses [29-32]. It should be noted that the dynamic responses of such footbridges are much more complicated and important than the static ones, especially when the static behaviour is pre-known. Luo et al. [33] proposed a hybrid finite element method to study the dynamic characteristics of the thin-walled box girder by considering the SLE. It was found that the natural frequencies considering the SLE have a general descending trend. Zhou et al. [34] theoretically investigated the dynamic characteristics of steel-concrete composite box beams considering the SLE and slip by introducing self-balancing of axial forces in a longitudinal warping function of beam section. Jiang et al. [35] studied the influence of high-order shear deformations and SLE on the dynamic characteristics of thin-walled box beams by using high-order beam theory. They concluded that the SLE increase with the increasing of mode order or the decreasing of span-width ratio. Cai et al. [36] derived the approximate solution of the first order vertical bending frequency for the simply supported curved thin-walled box girder considering the SLE. It has been reported that the SLE significantly affect the stiffness of the structures [35-36]. Zhang and Huang [37] proposed the analytical fundamental frequency of simply supported thin-walled box girder by using the energy variation principle method. Similarly, based on the energy variation principle method, Zhou et al. [38] analysed the influences of the SLE and shear deformation on the natural vibration characteristics of thin-walled box girder. Recently, Zhang et al. [39] investigated the SLE and accordion effect on dynamic characteristics of composite box girder bridge with corrugated steel web by proposing an analytical method. The aforementioned studies [35-39] indicate that the natural frequencies of the structures might be reasonably altered due to the SLE. However, the existing studies [33-39] on the dynamic responses of thin-walled box girder considering the SLE were mainly focused on the natural vibration characteristics or free vibration responses. To the best knowledge of the authors, however, there are very few studies related to SLE focusing on the forced vibrations of thin-walled box girder, not to mention the corresponding vibration control measures. In real world, human excitations are most relevant for footbridges. Thus, the pedestrian-induced vibration, as one of the most representative forced vibrations, is adopted to illustrate the influence of the SLE on the dynamic responses of the thin-walled box girder structure. Also, key parameters influencing the SLE are required to be identified. Furthermore, the effectiveness of the most often applied mitigation measures (TMD) should be investigated by considering the SLE. More importantly, to benefit footbridge designers, strategies are requested to consider the SLE on pedestrian-induced vibration and TMD-based vibration control of typical footbridges with thin-walled box section.

The remaining part of the paper is organized as follows. Section 2 briefly summarizes the theoretical framework of considering the SLE. Based on parametric study, the governing parameters are determined. Section 3 presents the simplified strategy of considering the SLE in the prediction of pedestrian-induced vibrations. The governing equations of motion are presented in the Section 4. Section 5 presents how the SLE affects the pedestrian-induced vibration levels of the structure. Section 6 discusses the influence of SLE on TMD-based vibration control of the structure. Conclusions are summarized in Section 7.

2. Shear lag effect

2.1 Basic assumptions

To illustrate the theoretical formulation of the SLE, a footbridge with typical thin-walled box section is firstly introduced (Fig. 1). According to a comprehensive review of more than 130 footbridges built after 1991 by [40], and the French guide Sétra [7] and the European guideline HiVoSS [8], it often applies simply supported beam model with sinusoidal mode shapes as the analytical model in calculating human-induced vibrations of footbridges. Therefore, the footbridge considered in this study is also idealized as a representative simply supported beam. In Fig. 1, L and W are the length and width of the bridge deck, respectively. H is the outer height of the box section. T_t, T_b, T_w are the thicknesses of top, bottom, and two vertical walls of the box section, respectively.

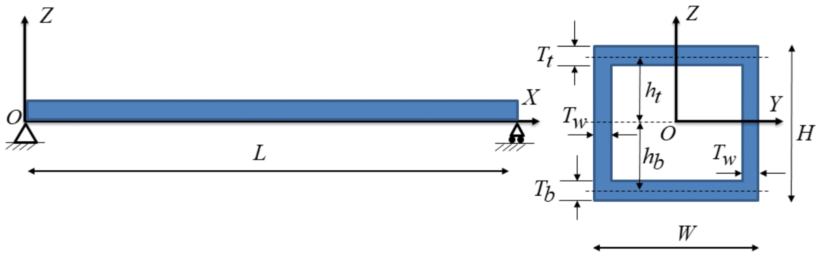

Fig. 1. The dimensions, cross section and coordinate system of the footbridge. The three directions are named as the longitudinal (X), the horizontal (Y), and the vertical (Z) directions.

The fundamental assumptions of the SLE include [35, 37-39]:

(1) The cross-sectional stiffness of the thin-walled section is not infinite and thus the cross section can deform both in and out of the plane. In the deformation process, the two vertical walls can basically remain in the plane and thus they are assumed to deform only in the plane.

(2) However, when the structure is deformed, the top and bottom walls have main movements in the X direction. The top and bottom walls' movements in the X direction can be expressed as parabolas along the Y direction.

(3) Considering the fact that the movements mainly exist in the X direction for the top and bottom walls, it assumes that the normal strain only exists in the X direction, i.e., $\varepsilon_x \neq 0$ and $\varepsilon_y = \varepsilon_z = 0$. Correspondingly, the shear strains are $\gamma_{yz} = \gamma_{xz} = 0$ and $\gamma_{yx} \neq 0$.

(4) To describe deformations of the cross section, displacement functions are introduced as: for the two vertical walls, the displacement in the Z direction is $w = w(x, t)$ (independent on y); for

the top and bottom walls, the displacements in the X direction are $u = u(x, y, t)$. The later can also be expressed as

$$u = u(x, y, t) = h[\frac{\partial w}{\partial x} + (1 - \frac{y^3}{b^3})\theta(x, t)] \quad (1)$$

with h the distance from the centroid of the cross section to the top wall h_t or to the bottom wall h_b. $b = (W - 2T_w)/2$ is half of the inner width of the cross section box. $\theta(x, t)$ is the rotational angle of the cross section. Based on its sinusoidal function-like shape, the rotational angle can be further expressed as

$$\theta(x, t) = \theta_0 \cos\left(\frac{\pi x}{L}\right) \sin(\omega t + \varphi) \quad (2)$$

The displacement in the Z direction with considering the SLE is similar to the case without considering the SLE, and thus it inherits the displacement function as

$$w = w(x, t) = w_0 \sin\left(\frac{\pi x}{L}\right) \sin(\omega t + \varphi) \quad (3)$$

2.2 Free vibration of footbridge with thin-walled box section considering SLE

The structure is assumed to be elastic when it is under free vibration. In addition, there is no additional energy input from the outside of the system. Thus, based on the Hamilton principle, it has:

$$\delta H = \delta \int_{t_0}^{t_1} (U - T) dt = 0 \quad (4)$$

where U and T are the strain energy and kinetic energy of the system, respectively. The strain energy can be obtained by

$$U = \frac{1}{2} \int \left[E(\varepsilon_x)^2 + G\left(\gamma_{yx}\right)^2\right] \mathrm{d}V \quad (5)$$

where E and G are elastic modulus and shear modulus, respectively; $\varepsilon_x = \frac{\partial u}{\partial x}$ and $\gamma_{yx} = \frac{\partial u}{\partial y}$.

The kinetic energy can be expresses as

$$T = \frac{1}{2} \int \int_0^L \rho (\frac{\partial w}{\partial L})^2 \, \mathrm{d}x\mathrm{d}A = \frac{1}{4} \rho A w_0^2 \omega^2 L[\cos(\omega t + \varphi)]^2 \quad (6)$$

Thus, for a duration of a full vibration period ($[0, \ 2\pi/\omega]$), substituting Eq. (5) and (6) into Eq. (4) yields

$$\delta H = \frac{\partial H}{\partial w_0} \delta w_0 + \frac{\partial H}{\partial u_0} \delta u_0 = 0 \quad (7)$$

Eq. (5) requires the following equation must be satisfied:

$$\begin{cases} \frac{\partial H}{\partial w_0} = 0 \\ \frac{\partial H}{\partial u_0} = 0 \end{cases} \tag{8}$$

and thus, it leads to the binary linear equations for w_0 and u_0.

By evaluating the corresponding determinant and obtaining non-zero roots, the fundamental natural circular frequency ω of the structure with considering the SLE can be derived, and the corresponding fundamental natural frequency is

$$f_{1,\mathrm{SLE}} = \frac{\omega}{2\pi} = (1-R)\left[\frac{\pi}{2}\sqrt{\frac{EI}{\bar{m}L^4}}\right] = (1-R)f_1 \tag{9}$$

where $f_1 = \frac{\pi}{2}\sqrt{\frac{EI}{\bar{m}L^4}}$ is the fundamental natural frequency of the structure without considering the SLE (the classic solution); $\bar{m} = \rho A = \rho[WH - (W - 2T_w)(H - T_t - T_b)]$ is the mass per unit length, with ρ the density of material; E is elastic modulus of material; I is moment of inertia of the cross section. Therefore, it theoretically obtains that the fundamental natural frequency for the case with considering the SLE has a reduction ratio R, and it is expressed as

$$R = \frac{35c_1}{40 + 28c_2c_3^2/\pi^2} \tag{10}$$

where the first coefficient c_1 reflects the contribution of moment of inertia from the top and bottom walls I_t and I_b, as

$$c_1 = \frac{I_t + I_b}{I} = \frac{\frac{1}{12}W(T_t)^3 + WT_t(h_t)^2 + \frac{1}{12}W(T_b)^3 + WT_b(h_b)^2}{\frac{1}{12}WH^3 - \frac{1}{12}(W - 2T_w)(H - T_t - T_b)^3} \tag{11}$$

The second coefficient c_2 is the ratio of the shear modulus to the Young's modulus and it is dependent on the Poisson's ratio ν, i.e.,

$$c_2 = \frac{G}{E} = \frac{1}{2(1+\nu)} \tag{12}$$

The last coefficient c_3 is related to the span-width ratio

$$c_3 = \frac{L}{2b} = \frac{L}{W - 2T_w} \tag{13}$$

with $2b$ the inner width of the cross section box.

Similarly, the natural frequency of the n^{th} mode for the structure with considering the SLE can also be obtained by introducing the reduction ratio:

$$f_{n,\mathrm{SLE}} = (1-R)[\frac{\pi n^2}{2}\sqrt{\frac{EI}{\bar{m}L^4}}] \tag{14}$$

2.3 Parametric study

Based on the theoretical solutions, the main governing parameters can be determined. In this subsection, the influences of four dimensionless parameters, i.e., span-width ratio, section thickness-width ratio, height-width ratio and Poisson's ratio, on the fundamental natural frequency and the corresponding reduction ratio R of the footbridge are presented. The footbridge with typical thin-walled box section shown in Fig. 1 is adopted as the benchmark structure for the parametric analysis. The dimensions of the benchmark footbridge are tabulated in Table 1. The Poisson's ratio of the benchmark structure is 0.30.

Table 1 The dimensions of the benchmark footbridge (unit: m)

L	W	H	T_t	T_b	T_w
50	3	3	0.1	0.1	0.1

2.3.1 Influence of span-width ratio

Different span-width ratios are presented by varying the typical spans from 25 m to 100 m while the width remains 3 m. Fig. 2 shows the fundamental natural frequencies and reduction ratios for different span-width ratios. In Fig. 2(a), the cases of 'with SLE', 'w/o SLE' and 'FEM solution' represent the scenarios of the theoretical solutions with and without considering the SLE and the Finite Element Method (FEM)-based numerical solution using the finite element software ANSYS V15.0, respectively. More specifically, for the FEM-based solutions, the BEAM188 element is adopted in ANSYS, then the cross section of the structure can be assumed to be infinite in the cross-sectional stiffness, which is similar to the case without considering the SLE. In the comparisons, the FEM-based solutions adopt four typical spans 25 m, 50 m, 75 m and 100 m. As shown in Fig. 2(a), with the increasing of the span-width ratio, the fundamental natural frequency decreases. The reduction of the natural frequencies due to the SLE becomes less and less significant with the increase of the span-width ratio, i.e. the reduction ratio is gradually approaching 0, as shown in Fig. 2(b). It implies that the SLE is more significant for footbridges with smaller span-width ratio. The comparison between 'w/o SLE' and 'FEM solution' in Fig. 2(a) also validates the theoretical solution for the case without considering the SLE. In reality, the cross-sectional stiffness is not infinite, and the cross section has the ability to deform both in and out of the plane. In other words, when the SLE is considered, the cross section is less stiff than the case of the beam model. It explains the decrease in natural frequency when the SLE is considered.

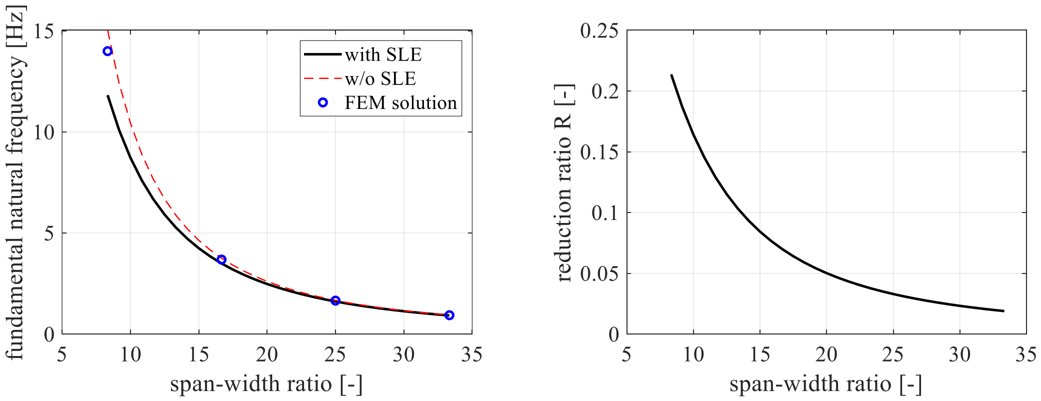

(a) (b)

Fig. 2. Variation of fundamental natural frequency and reduction ratio with respect to span-width ratio: (a) fundamental natural frequency; (b) reduction ratio.

2.3.2 Influence of section thickness-width ratio

Different section thickness-width ratios are illustrated by varying the typical section thickness from 0.05 m to 0.40 m while the width remains 3 m. Fig. 3 presents the fundamental natural frequencies and reduction ratios for different section thickness-width ratios. Fig. 3(a) clearly illustrates that the fundamental natural frequency linearly decreases with the increase of the section thickness-width ratio. When the SLE is considered, the fundamental natural frequencies are reduced. Fig. 3(b) further indicates that the reduction ratio decreases with the increase of the section thickness-width ratio. Therefore, the SLE is more significant for the footbridge with smaller section thickness-width ratio.

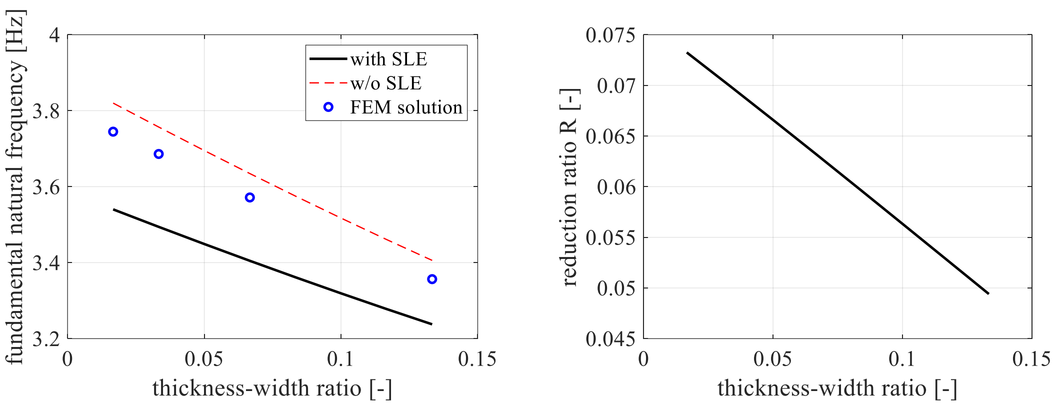

(a) (b)

Fig. 3. Variation of fundamental natural frequency and reduction ratio with respect to section thickness-width ratio: (a) fundamental natural frequency; (b) reduction ratio.

2.3.3 Influence of height-width ratio

Different height-width ratios are shown by varying the heights from 1.5 m to 6.0 m while the width remains 3 m. Fig. 4 depicts the fundamental natural frequencies and reduction ratios for different height-width ratios. It can be drawn from Fig. 4(a) that with the increasing of the height-width ratio, the fundamental natural frequency increases. The fundamental natural frequencies for the case with considering the SLE are lower than the case without considering the SLE. Fig. 4(b) shows that the reduction ratio decreases with the increase of the height-width ratio. Therefore, the SLE is more significant for the footbridge with lower height-width ratio.

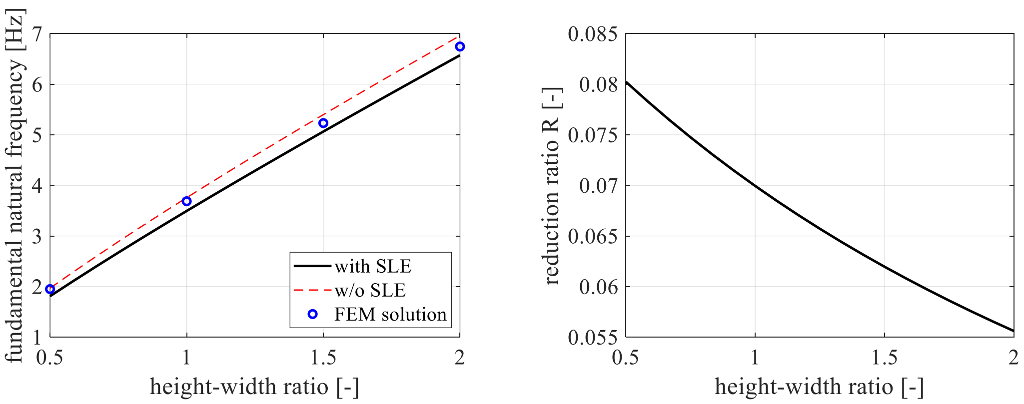

(a) (b)

Fig. 4. Variation of fundamental natural frequency and reduction ratio with respect to height-width ratio: (a) fundamental natural frequency; (b) reduction ratio.

2.3.4 Influence of Poisson's ratio

Different Poisson's ratios for typical footbridge materials, e.g., concrete and steel, are considered with the range of [0.20, 0.35]. Fig. 5 provides the fundamental natural frequencies and reduction ratios for different Poisson's ratios. Fig. 5(a) indicates that for the case without considering the SLE, the Poisson's ratio has negligible effect on the fundamental natural frequency; while for the case with considering the SLE, the fundamental natural frequency slightly decreases with the increase of the Poisson's ratio. Fig. 5(b) shows that the reduction ratio increases with the increase of the Poisson's ratio. It demonstrates that the SLE is more significant for the steel footbridge with larger Poisson's ratio than the concrete footbridge with smaller Poisson's ratio.

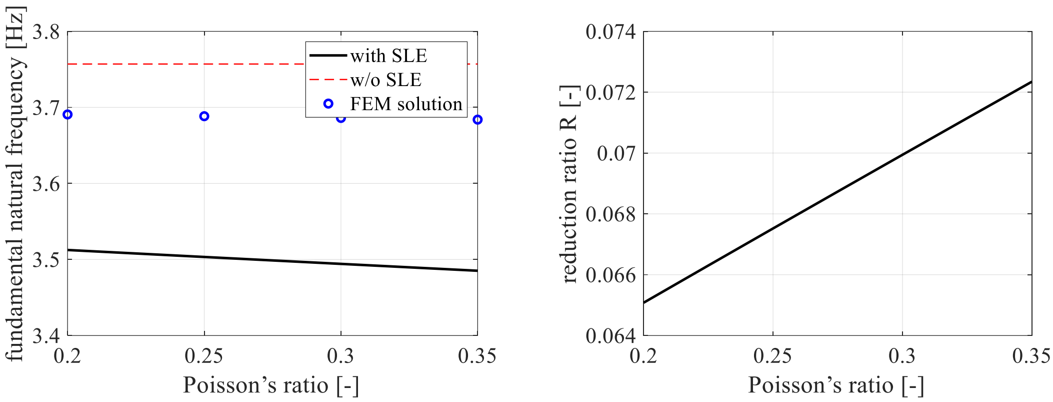

(a) (b)

Fig. 5. Variation of fundamental natural frequency and reduction ratio with respect to Poisson's ratio: (a) fundamental natural frequency; (b) reduction ratio.

2.3.5 Conclusions of parametric study

The above parametric analysis demonstrates that the natural frequencies of the footbridge can be significantly altered by considering the SLE. When being modelled in FEM software (e.g., ANSYS), the natural frequencies for the case 'with SLE' will be closer to the predicted values by the FEM model with shell element, which allows the cross section to deform both in and out of the plane. On the contrary, the results for the case 'w/o SLE' are nearer to the predicted results by the FEM model with beam element, i.e., the cross section only can deform in the plane due to assumed infinite cross-sectional stiffness. In other words, when the SLE is considered, the cross section is less stiff than the case of the beam model. It explains the decrease in natural frequency when the SLE is considered. Comparisons between the calculated results using Eqs. (9-14) and the predicted results of FEM models can also be applied to validate the theoretical solutions for the case with SLE. To sum up, the footbridges with smaller span-width ratios, smaller section thickness-width ratios, smaller height-width ratios and larger Poisson's ratios are more necessary to take the SLE into consideration. These uncertainties in the predicted natural frequencies due to the SLE may further result in inaccuracy in the prediction of pedestrian-induced vibrations of the footbridges.

3. Simplified strategy of considering SLE

As demonstrated in Section 2, the key task of considering the SLE is to determine the reduction ratio R. To consider the SLE on pedestrian-induced vibration and TMD-based vibration control of footbridges with thin-walled box section, for typical footbridges with different span-width ratios, section thickness-width ratios, height-width ratios and Poisson's ratios, the reduction ratio can be determined by referring the contour lines of the reduction ratios over different combinations of the governing parameters as determined in Section 2. The main procedures of the simplified strategy of considering the SLE are as follows.

(1) Pre-formulate the contour lines of the reduction ratios over different combinations of the governing parameters of the SLE in terms of natural frequency, as shown in Fig. 6. It can be conducted based on detailed parametric analysis using the analytical solutions of the SLE in Section 2. The corresponding simulations are only required to be done once for further applications. Thus, it is efficient and effective.

(2) Collect the governing parameters for the considered footbridge, i.e., span-width ratio, section thickness-width ratio, height-width ratio, and Poisson's ratio. These parameters can be conveniently obtained, e.g., from the plan of the footbridge.

(3) Determine the reduction ratio R for the considered footbridge from the pre-formulated contour lines by using the governing parameters.

(4) Obtain the natural frequencies of the structure without considering the SLE f_n based on the FEM using the beam element, or directly use the solutions based on the classical beam theory for typical beam-like footbridges, i.e. $f_n = \frac{\pi n^2}{2}\sqrt{\frac{EI}{\bar{m}L^4}}$, where n is the dominating mode. It is notable that FEM analysis based on beam element is much more computationally efficient than shell modelling. Thus, the proposed simplified strategy provides an efficient way to consider SLE by the reduction ratio R.

(5) Determine the natural frequencies of the structure with considering the SLE $f_{n,\mathrm{SLE}}$ by using Eq. (14).

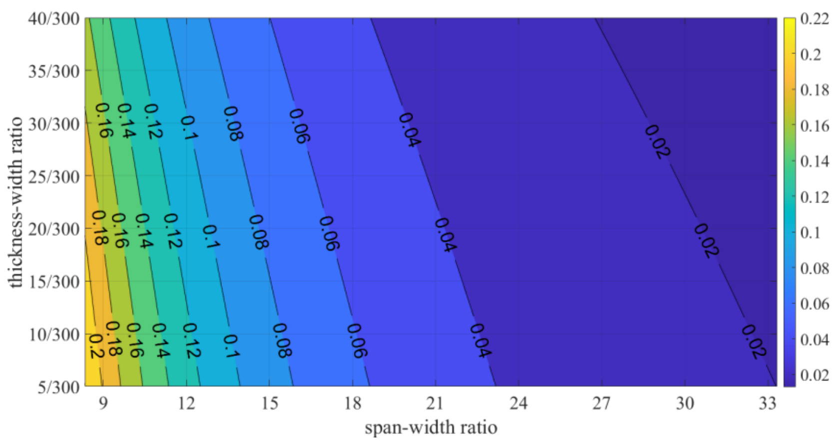

(a)

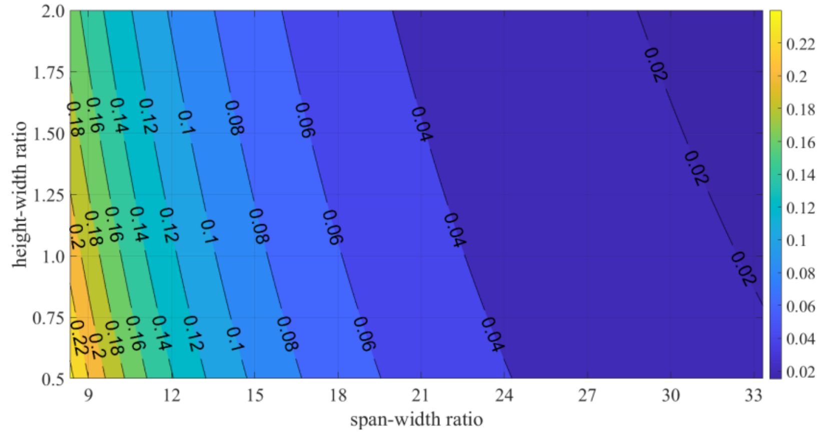
height-width ratio
span-width ratio

(b)

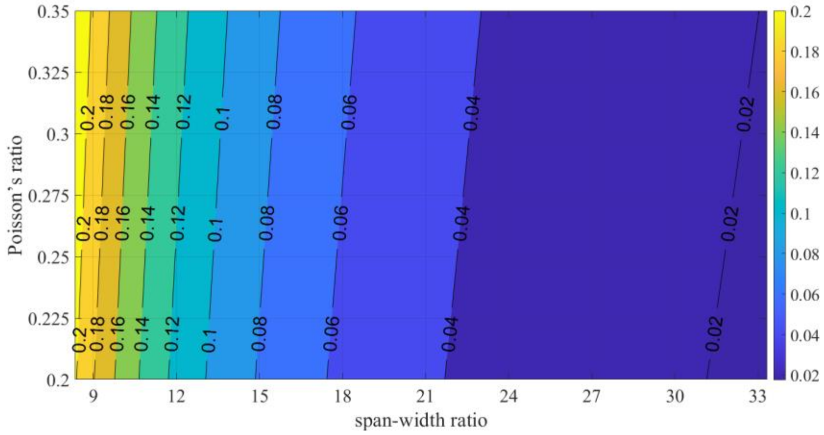
Poisson's ratio
span-width ratio

(c)

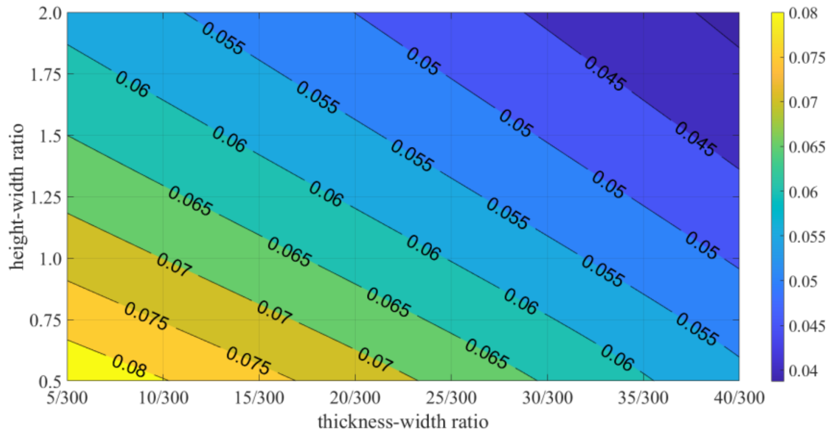
height-width ratio
thickness-width ratio

(d)

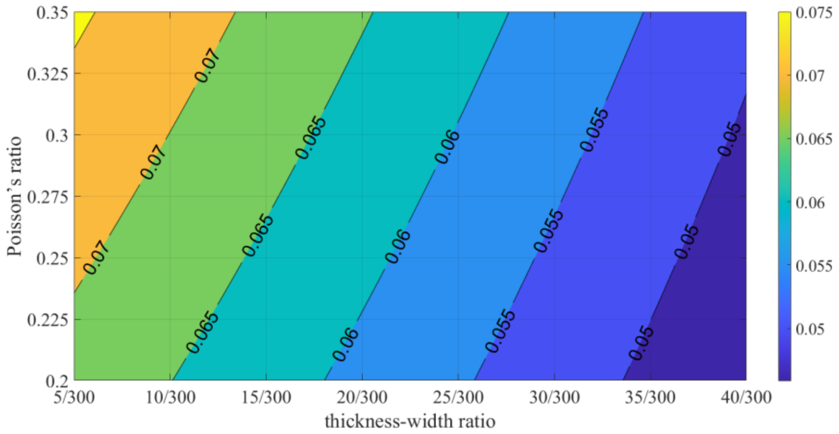

(e)

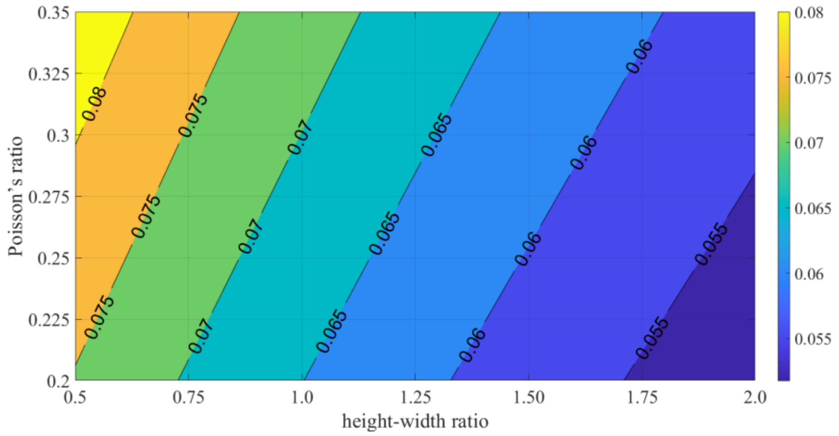

(f)

Fig. 6. Pre-formulated contour lines of the reduction ratios over different combinations of the governing parameters of the SLE in terms of natural frequency: An illustrative example for (a) height-width ratio = 1.0 and Poisson's ratio = 0.30; (b) section thickness-width ratio = 10/300 and Poisson's ratio = 0.30; (c) height-width ratio = 1.0 and section thickness-width ratio = 10/300; (d) span-width ratio = 50/3 and Poisson's ratio = 0.30; (e) span-width ratio = 50/3 and height-width ratio = 1.0; (f) span-width ratio = 50/3 and section thickness-width ratio = 10/300.

4. Calculation of pedestrian-induced vibration of footbridges

4.1 Pedestrian-Structure system

According to the design guidelines such as Sétra [7] and HiVoSS [8], the structural responses of footbridges are often dominated by one mode of the structure, of which the natural frequency is close to the pedestrian-induced excitations. For a pedestrian-structure system, the governing equation of motion can be expressed as:

$$m_{\text{Bridge}}\ddot{z}_{\text{Bridge}} + c_{\text{Bridge}}\dot{z}_{\text{Bridge}} + k_{\text{Bridge}}z_{\text{Bridge}} = F_{\text{ped}}(t)\phi(x) \tag{15}$$

where m_{Bridge}, $c_{\text{Bridge}} = 2m_{\text{Bridge}}\zeta_{\text{Bridge}}(2\pi f_{\text{Bridge}})$ and $k_{\text{Bridge}} = m_{\text{Bridge}}(2\pi f_{\text{Bridge}})^2$ are the corresponding modal mass, damping and stiffness coefficients of the bridge, respectively, in which f_{Bridge} and ζ_{Bridge} are the natural frequency and damping ratio of the bridge, respectively; $\ddot{z}_{\text{Bridge}}$, $\dot{z}_{\text{Bridge}}$ and z_{Bridge} are the modal acceleration, velocity and displacement of the bridge, respectively; $F_{\text{ped}}(t)$ is the pedestrian-induced force; $\phi(x)$ is the corresponding vibration mode.

The pedestrian-induced forces induced by single person are considered by taking the dominating harmonic of the largest component of the walking force as follows:

$$F_{\text{walk,}z}(t)/G_{\text{ped}} = 1 + DLF_z \sin(2\pi f_{\text{ped}} t + \varphi_z) \tag{16}$$

where $F_{\text{walk,}z}(t)$ is the pedestrian induced walking force in the vertical (Z) direction of the bridge deck (Fig. 1), respectively; G_{ped} is the pedestrian's weight; DLF_z is the corresponding dynamic load factor (DLF) in the vertical (Z) direction; f_{ped} is the walking step frequency; φ_z is the phase angle in the vertical (Z) direction. All these parameters are diverse for different individuals because of the inter-subject variability and they are not even always the same for the same person due to the intra-subject variability.

In this study, to illustrate the effects of SLE on pedestrian-induced vibrations, the walking force model is considered in two different ways as follows.

(1) A deterministic model: to keep the model as realistic and simple as possible in investigating the SLE, a deterministic set of values is firstly applied, e.g. as proposed/applied in [41-42]: $G_{\text{ped}} = 800$ N, $DLF_z = 0.4$, $f_{\text{ped}} = 2$ Hz, and $\varphi_z = 0$. When necessary, to calculate the maximum peak acceleration response, the step frequency f_{ped} can be set to the resonant frequency.

(2) A probabilistic model: to consider the inter- and intra-subject variability of walking forces, the pedestrian weight G_{ped} is considered as a normal distribution, e.g. with a mean of 800 N and a variation coefficient of 10%. Step frequency f_{ped} follows a normal distribution, e.g. with a mean of 2 Hz and a standard deviation of 0.173 Hz, according to Matsumoto et al. [43]. When the maximum peak acceleration response is interested, the mean step frequency can be set to the resonant frequency as it does in the deterministic model. According to Young [44-45], the dynamic load factors in the vertical depends on step frequency as: $DLF_z = 0.41(f_{\text{ped}} - 0.95)$, in which f_{ped} in [1, 2.8] Hz. Due to the lack of reliable experimental data and explicit physical meaning, the phase angles

are kept as $\varphi_z = 0$. For a continuous pedestrian flow, the arrival times of different persons in the crowd are normally considered as a Poisson process, e.g. as applied in [2].

Fig. 7 presents the vertical component of the normalized walking force, which is defined as the ratio of the walking force to the pedestrian's weight, in accordance with the applied deterministic set of parametric values. Fig. 7 further indicates that the vertical component of the walking force fluctuates near the body weight, with the maximum amplitude of $(1 + DLF_z) \cdot G_{\mathrm{ped}}$. Correspondingly, the modal loads for the deterministic model are obtained by multiplying the walking forces with the mode shapes. For a sinusoidal mode shape, the modal loads are maximum when the pedestrian is walking at the midspan of the structure; while they become zero before the person's arrival on and after the person's left off the bridge.

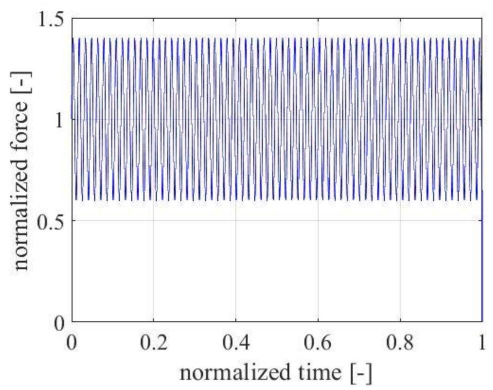

Fig. 7. The considered normalized walking forces of the deterministic model.

4.2 Reduction of pedestrian-induced vibration using TMD

To reduce the pedestrian-induced vibration of civil structures, installation of the TMD is a widely-applied and effective approach [46-47]. In the pedestrian-structure system with a TMD shown in Fig. 8, m_{TMD}, $c_{\mathrm{TMD}} = 2m_{\mathrm{TMD}}\zeta_{\mathrm{TMD}}(2\pi f_{\mathrm{TMD}})$ and $k_{\mathrm{TMD}} = m_{\mathrm{TMD}}(2\pi f_{\mathrm{TMD}})^2$ are the mass, damping and stiffness coefficients of the TMD; in which f_{TMD} and ζ_{TMD} are the natural frequency and damping ratio of the TMD, respectively.

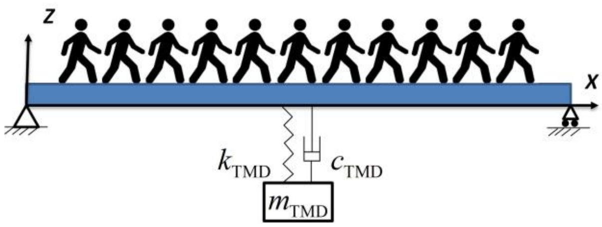

Fig. 8. A pedestrian-structure system with a TMD.

The governing equations of motion for the pedestrian-structure system with a TMD are:

$$m_{\mathrm{Bridge}}\ddot{z}_{\mathrm{Bridge}} + c_{\mathrm{Bridge}}\dot{z}_{\mathrm{Bridge}} + k_{\mathrm{Bridge}}z_{\mathrm{Bridge}} - c_{\mathrm{TMD}}\left(\dot{z}_{\mathrm{TMD}} - \dot{z}_{\mathrm{Bridge}}\right) - k_{\mathrm{TMD}}\left(z_{\mathrm{TMD}} - z_{\mathrm{Bridge}}\right) = F_{\mathrm{ped}}(t)\phi(x) \quad (17)$$

$$m_{\mathrm{TMD}}\ddot{z}_{\mathrm{TMD}} + c_{\mathrm{TMD}}\left(\dot{z}_{\mathrm{TMD}} - \dot{z}_{\mathrm{Bridge}}\right) + k_{\mathrm{TMD}}\left(z_{\mathrm{TMD}} - z_{\mathrm{Bridge}}\right) = 0 \quad (18)$$

where $\ddot{z}_{\mathrm{TMD}}$, $\dot{z}_{\mathrm{TMD}}$ and z_{TMD} are the acceleration, velocity and displacement of the TMD, respectively.

To determine the design parameters of the TMD, resonant conditions are assumed, i.e., resonance with the targeted mode where the TMD is tuned is assumed. Furthermore, mass ratio γ_M and frequency ratio γ_F are introduced. Mass ratio γ_M is defined as the ratio of the TMD mass m_{TMD} to the bridge mass m_{Bridge}. Similarly, frequency ratio γ_F is defined as the ratio of the TMD frequency f_{TMD} to the bridge frequency f_{Bridge}. For a given mass ratio γ_M, Den Hartog [48] provided the classical solution for determining the optimal TMD parameters by minimising the maximum displacement response of the structure, i.e.,

$$\gamma_F = \frac{f_{\mathrm{TMD}}}{f_{\mathrm{Bridge}}} = \frac{1}{1+\gamma_M} \quad (19)$$

$$\zeta_{\mathrm{TMD}} = \sqrt{\frac{3\gamma_M}{8(1+\gamma_M)}} \quad (20)$$

Then, the optimal TMD parameters are summarized as follows:

$$m_{\mathrm{TMD}} = \gamma_M m_{\mathrm{Bridge}} \quad (21)$$

$$c_{\mathrm{TMD}} = 2m_{\mathrm{TMD}}\zeta_{\mathrm{TMD}}(2\pi f_{\mathrm{TMD}}) = \frac{4\pi\gamma_M}{1+\gamma_M}\sqrt{\frac{3\gamma_M}{8(1+\gamma_M)}}\, m_{\mathrm{Bridge}} f_{\mathrm{Bridge}} \quad (22)$$

$$k_{\mathrm{TMD}} = m_{\mathrm{TMD}}(2\pi f_{\mathrm{TMD}})^2 = \frac{4\pi^2\gamma_M}{(1+\gamma_M)^2} m_{\mathrm{Bridge}}\left(f_{\mathrm{Bridge}}\right)^2 \quad (23)$$

It can be seen from the above equations that all the three parameters of the TMD are dependent on the mass ratio γ_M, which is determined by the designer.

4.3 Flowchart of calculating pedestrian-induced vibration of footbridges

For a footbridge subjected to pedestrian-induced excitations, i.e., a pedestrian-structure system, the structural responses can be obtained by solving the governing equation of motion (Eq. 15) and the walking force model in the subsection 4.1. The footbridge can be simulated by FEM using the beam element or the simplified mathematic model, i.e., structural equation of motion. Then, the fundamental natural frequency of the footbridge f_1 (f_{Bridge}) without considering the SLE can be obtained. Next, the fundamental natural frequency of the footbridge $f_{1,\mathrm{SLE}}$ (f_{Bridge}) with considering the SLE can be calculated by using Eq. (9) or the simplified strategy indicated in Section 3. Based on f_1 or $f_{1,\mathrm{SLE}}$, the parameters of the TMD can be respectively determined by using the design method presented in the subsection 4.2. As a result, the installation of the TMD into the pedestrian-structure system forms a new coupled system, i.e., the pedestrian-TMD-structure system, which has two different sets of parameter values, corresponding to the two cases without and with considering the SLE. The structural responses of them can be obtained by solving the governing equation of motion (Eq. 17) and the walking force model in the subsection 4.1. Fig. 9 illustrates the flowchart of calculating the pedestrian-induced vibration of footbridges.

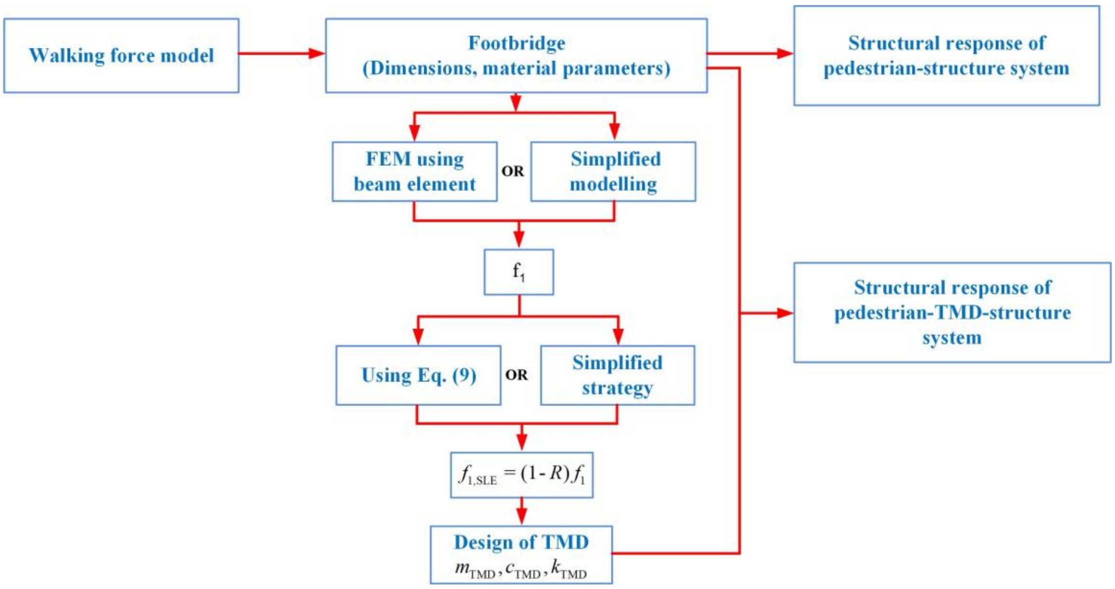

Fig. 9. Flowchart of calculating pedestrian-induced vibration of footbridges.

5. Influence of SLE on pedestrian-induced vibration

5.1 Structural parameters

The footbridge with typical thin-walled box section shown in Fig. 1 is adopted as the example structure. The length L of the considered structure is 70 m, while other dimensions of the footbridges are inherited from Table 1. The material properties are also the same as those of the benchmark structure in the subsection 2.3. The corresponding damping ratio is assumed to be 0.5%. The modal mass is considered as 50 tons for the example structure. According to the simplified strategy (Section 3), considering the span-width ratio (70/3), section thickness-width ratio (10/300), height-width ratio (3/3), and Poisson's ratio (0.3), the reduction ratio R of the fundamental frequency can be obtained from the pre-formulated contour lines as 3.76%. The fundamental frequency without considering SLE can be calculated based on the beam theory, i.e. $f_1 = 1.9168$ Hz. Then, the value for the case with SLE is determined as $f_{1,\mathrm{SLE}} = 1.8448$ Hz. These parameters are applied for further analysis.

5.2 Structural responses

5.2.1 Results based on the deterministic force model

Fig. 10 shows the time history of the induced structural responses during the pedestrian passing the bridge with a walking speed of 1.5 m/s for the example structure with the length of 70 m. As shown in Fig. 10, large discrepancies are observed in the prediction of the pedestrian-induced vibrations of the footbridges with and without considering the SLE. For the special case in Fig. 10, the peak acceleration without considering the SLE is approximately twice that of the case with considering the SLE. For broad applications in the vibration serviceability, the inaccuracy/unreliable predictions of pedestrian-induced vibrations may be caused when the actual natural frequency should be $f_{1,\mathrm{SLE}}$, which is however considered as f_1 due to without considering the SLE.

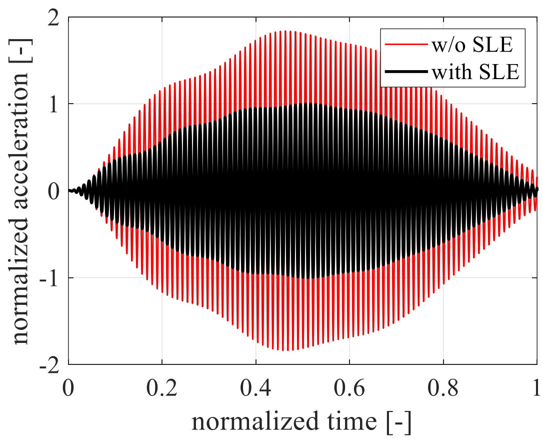

Fig. 10. Time history of the induced structural responses during the pedestrian passing the bridge.

Fig. 11 further illustrates the peak acceleration ratios of the case without considering the SLE to the case with considering the SLE for the induced structural responses during the pedestrian passing the bridge for different span-width ratios, section thickness-width ratios, height-width ratios and Poisson's ratios, respectively. It can be drawn from Fig. 11 that:

(1) Fig. 11(a): When the span-width ratio is lower than 23, without considering the SLE results in lower vibration responses; while when the span-width ratio is higher than 23, without considering the SLE results in higher vibration responses. For large span-width ratios, with the increase of the span-width ratio, the peak acceleration ratio approaches to 1. This can be explained by the variation of fundamental natural frequencies for different span-width ratios (Fig. 2). For instance, when the span-width ratio is close to 23, the natural frequency (e.g. for the example structure, the span-width ratio is 23.33, with corresponding $f_{1,\mathrm{SLE}} = 1.8448$ Hz and $f_1 = 1.9618$ Hz) is approaching the excitation frequency 2 Hz, it may result in very sensitive changes in structural responses even if there are relatively small changes in natural frequency.

(2) Fig. 11(b): With the increase of the section thickness-width ratio, the peak acceleration ratio increases but not more than 1. It means that the predicted structural responses are lower for the case without considering the SLE than the case with considering the SLE, of which the natural frequency is closer to the excitation frequency (Fig. 3).

(3) Fig. 11(c): With the increase of the height-width ratio, the peak acceleration ratio approaches to 1, which means the SLE becomes insignificant. It also should be noted that when the height-width ratio is 0.5, the predicted structural responses for the case without considering the SLE are much higher than the case with considering the SLE due to the near-resonance for the case without considering the SLE (Fig. 4).

(4) Fig. 11(d): The effect of Poisson's ratio on the peak acceleration ratio is relatively insignificant, which results from that the fundamental natural frequency does not vary much with the Poisson's ratio (Fig. 5).

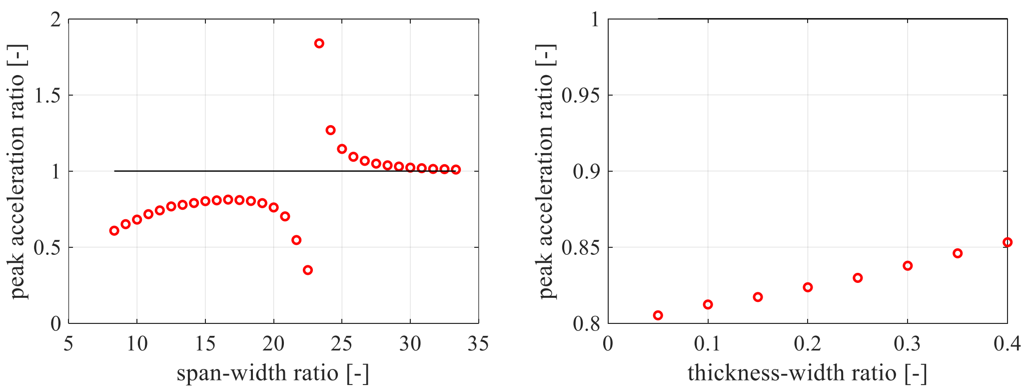

(a) (b)

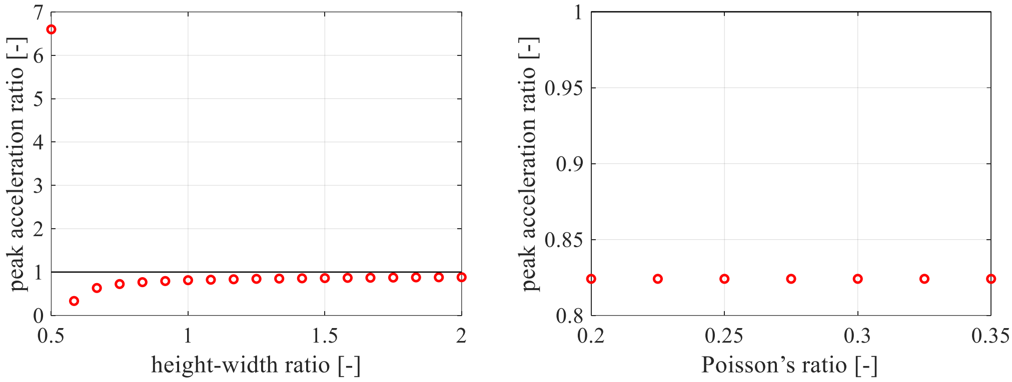

(c) (d)

Fig. 11. Peak acceleration ratio (the case without SLE to the case with SLE) of the induced structural responses during the pedestrian passing the bridge for different (a) span-width ratios, (b) section thicknesses, (c) height-width ratios, and (d) Poisson's ratios.

5.2.2 Results based on the probabilistic force model

To consider the inter- and intra-subject variability of walking forces, large number of persons with different parametric values in accordance with the probabilistic model are adopted in the study (as discussed in the subsection 4.1). Fig. 12 compares the induced structural responses by different persons, in terms of non-exceedance probability of the peak acceleration ratio. Several conclusions can be drawn from Fig. 12 and as follows:

(1) For different span-width ratios (Fig. 12(a)), the majority of peak acceleration ratios are near or lower than 1, i.e., without considering the SLE, the predicted structural responses are probably lower than the actual case with considering the SLE. It should be noted that the peak acceleration ratio can even reach to 6. It means that considering the SLE also might result in much higher structural responses in predictions. In addition, the SLE becomes insignificant for the cumulative probability range of [0.5, 0.9] as the peak acceleration ratios are close to 1.

(2) For different height-width ratios (Fig. 12(c)), over 80% of the peak acceleration ratios are near the value of 1. In other words, the SLE is insignificant for most cases. However, the remaining less than 20% cases can be very significant because the peak acceleration ratios can reach either 0 or over 10.

(3) The effects of section thickness-width ratio and Poisson's ratio are not very significant, resulting in very narrow ranges for the peak acceleration ratios with values slightly lower than 1 (Fig. 12(b) and (d)).

(4) The SLE on the prediction of pedestrian-induced vibrations are mainly dependent on the ratio of the excitation frequency to the structural natural frequency. When the excitation frequency and the structural natural frequency are close, the SLE becomes significant. This results from that the induced acceleration amplitudes mainly depend on the excitation frequency and the structural natural frequency. In addition, the changes in structural responses may be very sensitive to even relatively small changes in the structural natural frequency due to the SLE.

All these results also confirm the necessity of considering the SLE in predicting the pedestrian-induced vibrations of the footbridges.

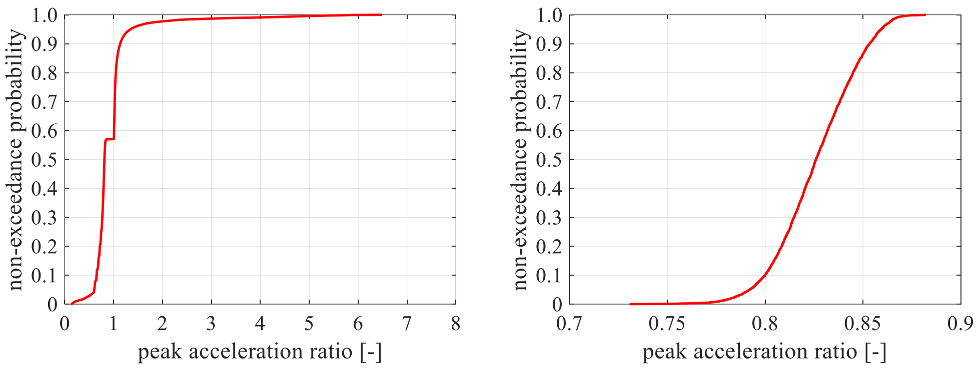

(a) (b)

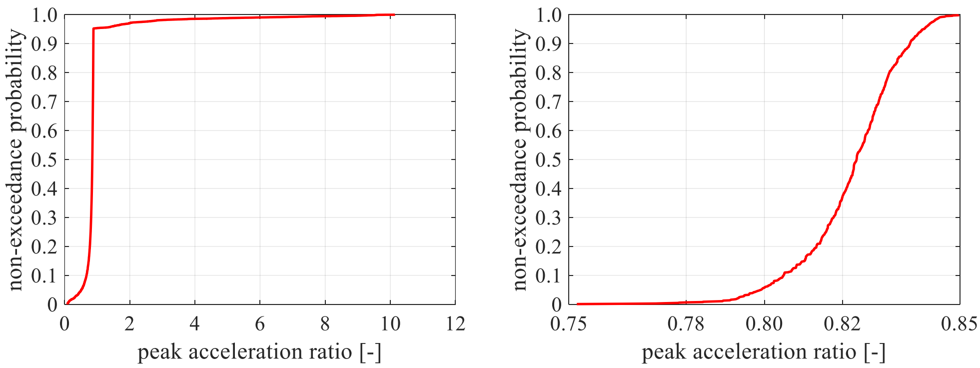

(c) (d)

Fig. 12. Comparison of induced structural responses by different persons in terms of peak acceleration ratios for different (a) span-width ratios, (b) section thickness-width ratios, (c) height-width ratios, and (d) Poisson's ratios.

6. Influence of SLE on TMD-based vibration control

6.1 TMD parameters

The TMD parameters are required to be tuned based on the actual modal parameters, i.e., the case with SLE ($f_{1,\mathrm{SLE}}$). Thus, design parameters of the TMD are different if the SLE is not considered (f_1). For the example structure, the mass ratio is considered as $\gamma_M = 0.01$. The TMD parameters can be determined by using Eqs. (19-23). As a result, when the TMD is designed based on the case without considering the SLE, the damping ratio and natural frequency of the TMD are $\zeta_{\mathrm{TMD}} = 0.0609$ and $f_{\mathrm{TMD}} = 1.8978$ Hz, respectively. For the actual case with considering the SLE, the damping ratio and natural frequency of the TMD are $\zeta_{\mathrm{TMD,SLE}} = 0.0609$ and $f_{\mathrm{TMD,SLE}} = 1.8265$ Hz, respectively. Other design parameters of the TMD are listed in Table 2.

Table 2 Design parameters of TMD

Case	Damping ratio	Frequency (Hz)	Mass (ton)	Damping (N·s/m)	Stiffness (N/m)
w/o SLE	0.0609	1.8978	0.5	726.6	7.11×10^4
with SLE	0.0609	1.8265	0.5	699.3	6.59×10^4

6.2 Structural responses

To quantify the damping effect of the TMD on the structural responses, reduction factor of the TMD R_{TMD} can be defined based on the reduction in the structural responses, as:

$$R_{\mathrm{TMD}} = 1 - \frac{\max|u_{\mathrm{with\ TMD}}|}{\max|u_{\mathrm{without\ TMD}}|} \tag{24}$$

where $u_{\mathrm{with\ TMD}}$ and $u_{\mathrm{without\ TMD}}$ are the structural responses (acceleration or displacement) with and without the TMD, respectively.

Fig. 13 shows the comparison of normalized acceleration and displacement time history curves of structural systems with and without the TMD for the example structure. It can be seen from Fig. 13 that the instalment of the TMD has excellent performance in mitigating structural responses.

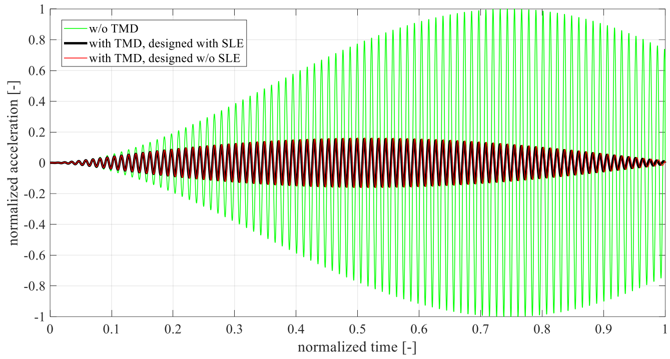

(a)

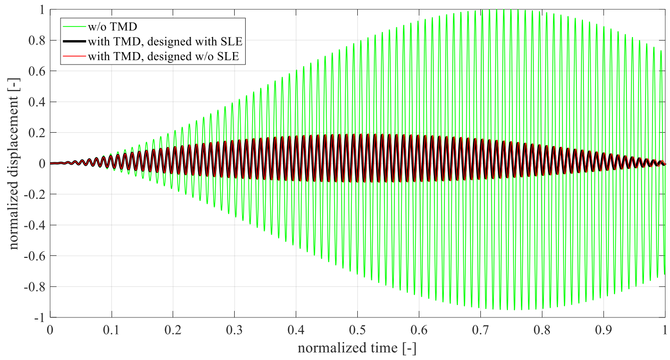

(b)

Fig. 13. Comparison of normalized acceleration and displacement time history curves of structural systems with TMD and without TMD for the example structure: (a) acceleration; (b) displacement.

Fig. 14 further compares structural responses of pedestrian-TMD-structure systems with and without considering the SLE for the example structure. As shown in Fig. 14, although there is merely 3.76% reduction in the structural natural frequency (1.9168 Hz vs. 1.8448 Hz) by considering the SLE, the damping effect of the TMD designed without considering the SLE is less superior as the TMD designed with considering the SLE. To be specific, the reduction factors R_{TMD} of acceleration responses for the cases without and with considering the SLE are 83.79% and 84.53%, respectively, while the reduction factors R_{TMD} of displacement responses for the cases without and with considering the SLE are 80.8% and 81.55%, respectively. When without SLE considering in the TMD design, the acceleration amplitude can only be reduced to 16.21% of the acceleration amplitude of the case without TMD installed, which is higher than 15.47% the case with SLE. The remained displacement amplitudes are about 19.20% and 18.45% of the displacement amplitude of the case without TMD installed for the case without and with SLE considered in the TMD design, respectively. Correspondingly, the effective damping ratio of the structure with TMD is reduced around 3.87%. It is notable that, although the reduction in the effective damping ratio is not incredibly significant for the considered structure, it already shows the negative effects of the SLE in the vibration mitigation. More significant effects will be illustrated in following paragraphs with other investigations.

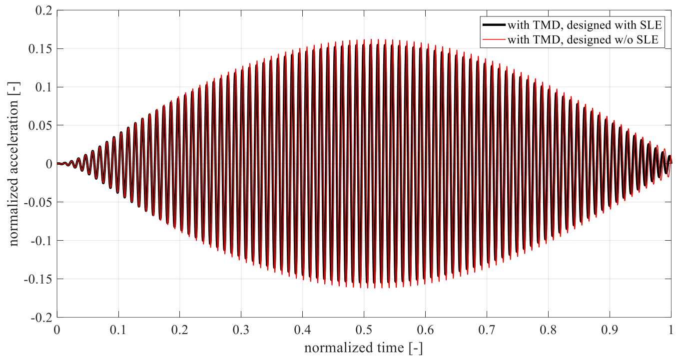

(a)

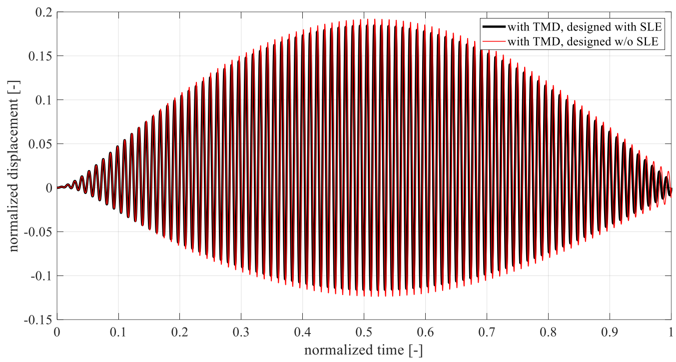

(b)

Fig. 14. Comparison of normalized acceleration and displacement time history curves of the pedestrian-TMD-structure system with and without considering the SLE for the example structure: (a) acceleration; (b) displacement.

For other cases, the difference between the reduction effects of the TMDs designed with and without considering the SLE might be more significant. To be quantified, the reduction factors R_{TMD} of acceleration and displacement responses for different span-width ratios, section thicknesses, height-width ratios, and Poisson's ratios are provided in Figs. 15 and 16, respectively. It can be found that the reduction factors R_{TMD} of acceleration and displacement responses have very similar trends. When the TMD is designed with considering the SLE, the reduction factors are constants. On the contrary, the reduction factors become variables when the TMD is designed without considering the SLE. The reduction factors of the TMD designed with considering the SLE are always larger than the corresponding TMD without considering the SLE. With the increasing of the span-width ratio, thickness-width ratio, height-width ratio, or the decreasing of the Poisson's ratio, the gap becomes smaller due to less significant SLE. In addition, the span-width ratio has the most significant influence on the differences of the reduction factors for two different TMDs. The thickness-width ratio and thickness-width ratio are less significant, and the influence of the Poisson's ratio is relatively insignificant. This is also validated by the plot of effective damping ratio of the system (Fig. 17). For instance, when the span-width ratio is smaller than 10, the reduction in the effective damping ratio can be over 50%. For different thickness-width ratios, height-width ratios, and Poisson's ratios, the largest reductions can only be around 20%. On the other hand, the reduction in effective damping capacity due to without considering SLE in the TMD-design result in less effective in the vibration mitigation.

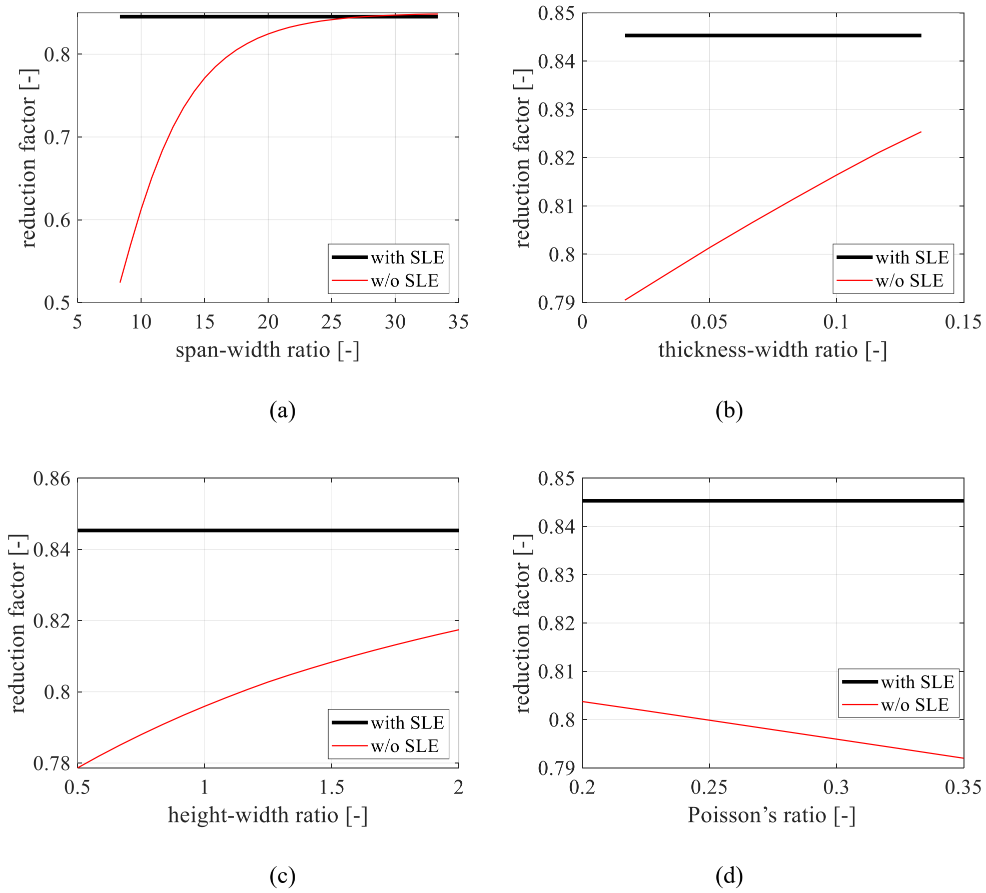

Fig. 15. Reduction factors of acceleration responses without and with considering the SLE for different (a) span-width ratios, (b) section thickness-width ratio, (c) height-width ratios, and (d) Poisson's ratios.

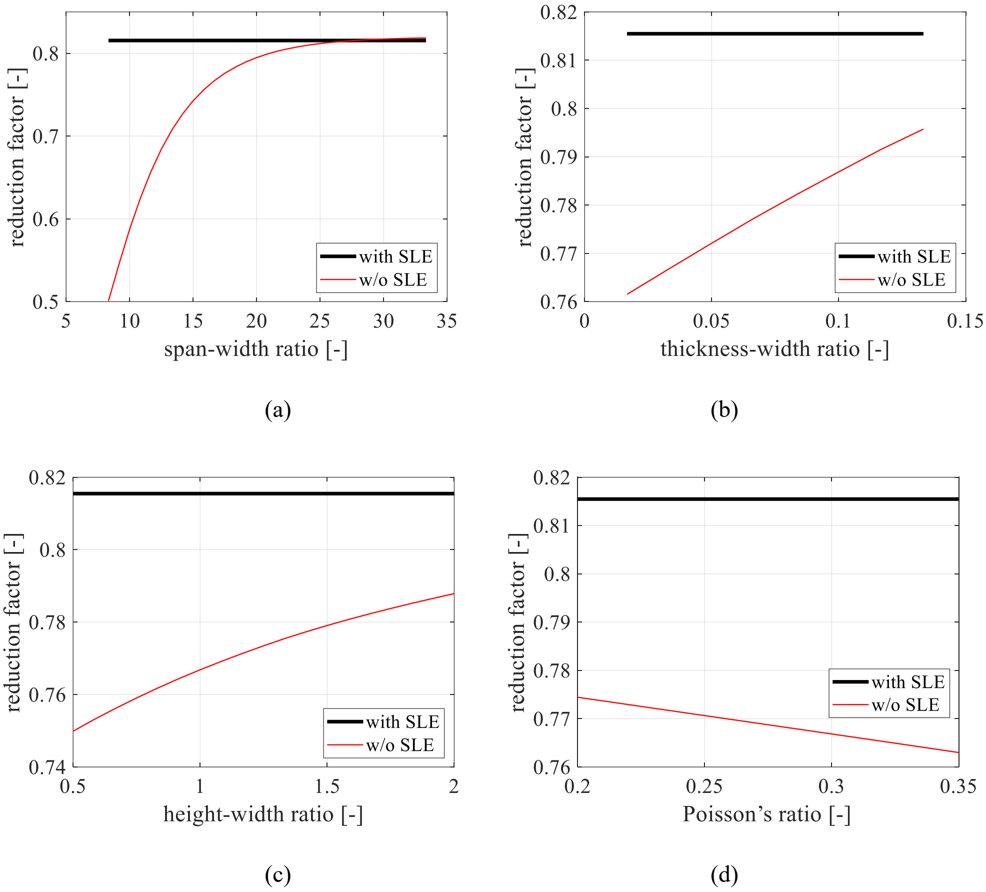

Fig. 16. Reduction factors of displacement responses without and with considering the SLE for different (a) span-width ratios, (b) section thickness-width ratio, (c) height-width ratios, and (d) Poisson’s ratios.

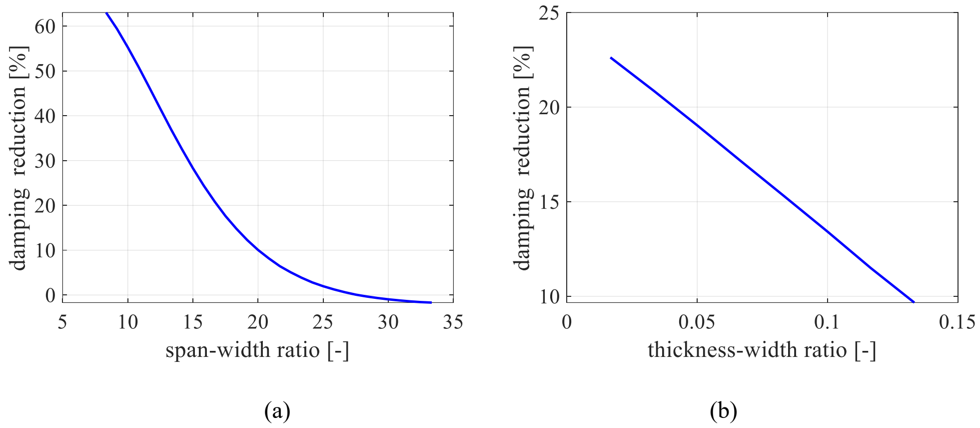

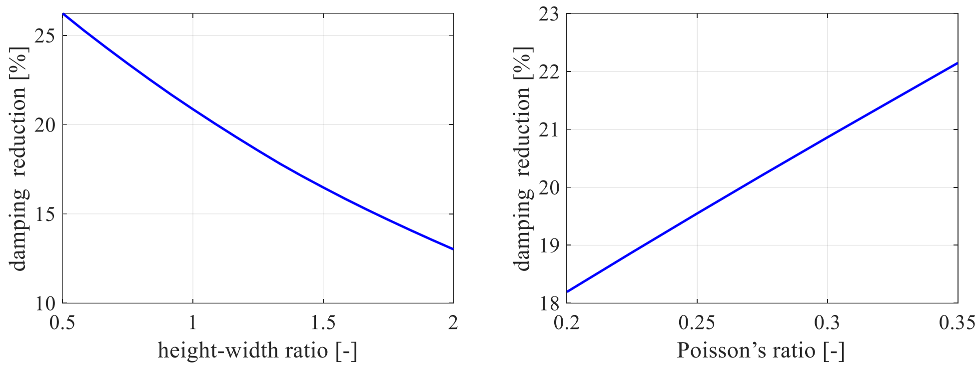

(c) (d)

Fig. 17. Reductions in the effective damping ratio due to the designed TMD without considering the SLE for different (a) span-width ratios, (b) section thickness-width ratio, (c) height-width ratios, and (d) Poisson's ratios.

7. Conclusions

This paper investigates the SLE on the pedestrian-induced vibration and TMD-based vibration control of typical footbridges with thin-walled box section, by providing the theoretical framework to consider the SLE on the natural frequencies of the structure. Furthermore, an efficient way to consider the SLE is proposed. The main conclusions are drawn as follows:

(1) The SLE on the natural frequencies of the structure can be considered with a reduction ratio to the corresponding case without considering SLE (the classic solutions of natural frequencies).

(2) The footbridges with smaller span-width ratios, smaller section thickness-width ratios, and lower height-width ratios are more necessary to consider the SLE. Furthermore, although the Poisson's ratio effects are relatively lower than other aspects, the steel bridges still need to be paid to attention for the SLE. Due to the SLE, it may result in significant reductions in the natural frequencies of the structures.

(3) These reductions in the predicted natural frequencies due to ignore the SLE may further result in significantly inaccuracy in the prediction of pedestrian-induced vibrations of the footbridges.

(4) Furthermore, the most often applied mitigation measures may not be reliably designed. Due to the fact that TMD is only effective in a narrow frequency range near the damped mode, TMD design needs to reliable modal parameters and thus requires considering the SLE in the TMD-based vibration control of footbridges with thin-walled box section.

Otherwise, it may result in very significant reduction in the effectiveness of the vibration mitigation measures.

The study is illustrated mainly based on typical footbridges with thin-walled box sections; however, the proposed methodology can be applied to the vibration serviceability analysis for all other footbridges.

Acknowledgments

Financial support from the National Natural Science Foundation of China (Grant Nos. 51908048, 52108432), the Young Talent Fund of University Association for Science and Technology in Shaanxi, China (Grant No. 20200412) are gratefully acknowledged.

References

[1] W. H. Hu, C. Moutinho, E. Caetano, et al, Continuous dynamic monitoring of a lively footbridge for serviceability assessment and damage detection, *Mech. Syst. Sig. Process*. 33 (2012) 38–55, http://dx.doi.org/10.1016/j.ymssp.2012.05.012.

[2] B. Fu and X. Wei, An intelligent analysis method for human-induced vibration of concrete footbridges. *Int. J. Struct. Stab. Dyn*. 21(1) (2021) 2150013. https://doi.org/10.1142/S0219455421500139.

[3] R. J. Ma, L. Ke, D. L. Wang, A. R. Chen and Z. C. Pan, Experimental study on pedestrians' perception of human-induced vibrations of footbridges, *Int. J. Struct. Stab. Dyn*. 18(10) (2018) 1850116.

[4] Ming Gong, Yunsheng Li, Ruili Shen and Xinxin Wei. Glass suspension footbridge: human-induced vibration, serviceability evaluation, and vibration mitigation. *Journal of Bridge Engineering*, 26 (11): 05021014. https://doi.org/10.1061/(ASCE)BE.1943-5592.0001788

[5] J. Chen, L. Wang, V. Racic, et al, Acceleration response spectrum for prediction of structural vibration due to individual bouncing, *Mech. Syst. Sig. Process*. 76-77 (2016) 394–408, http://dx.doi.org/10.1016/j.ymssp.2016.02.032.

[6] Stana Živanović and Aleksandar Pavić, Probabilistic Modeling of Walking Excitation for Building Floors, *Journal of Performance of Constructed Facilities*. 23(3), 2009. https://doi.org/10.1061/(ASCE)CF.1943-5509.0000005

[7] Sétra, Footbridges: assessment of vibrational behaviour of footbridges under pedestrian loading. *Afgc, Paris*, 2006, Available via: http://www.setra.equipement.gouv.fr.

[8] HiVoSS, Design of footbridges guideline. Human induced vibrations of steel structures, *2008. Retrieved from http://www.stb.rwth-aachen.de/projekte/2007/HIVOSS/download.php (RFS2-CT-2007-00033)*.

[9] L. Dai, N. Yang, Q. Yang, Bayesian prediction of structural response under crowd-induced walking load, *Int. J. Struct. Stab. Dyn*. 18(3) (2018) 1850039.

[10] B. Y. Jia, X. L. Yu, and Q. S. Yan, Effects of stochastic excitation and phase lag of pedestrians on lateral vibration of footbridges, *Int. J. Struct. Stab. Dyn*. 18(7) (2018) 1850095.

[11] Y. A. Gao, Q. S. Yang and Y. Dong, A three-dimensional pedestrian–structure interaction model for general applications, *Int. J. Struct. Stab. Dyn*. 18(9) (2018) 1850107.

[12] L. J. Ouyang, T. T. Li, B. Zhen and L. Wei, Dynamics of a pedestrian's walking motion based on the inverted pendulum model, *Int. J. Struct. Stab. Dyn*. 18(11) (2018) 1850145.

[13] Y. A. Gao and Q. S. Yang, A theoretical treatment of crowd–structure interaction, *Int. J. Struct. Stab. Dyn*. 18(1) (2018) 1871001.

[14] X. Wei, J. Liu, S. Bi, Uncertainty quantification and propagation of crowd behaviour effects on pedestrian-induced vibrations of footbridges, *Mechanical Systems and Signal Processing*, 167 (Part A): 108557, https://doi.org/10.1016/j.ymssp.2021.108557.

[15] F. Venuti, A. Reggio, Mitigation of human-induced vertical vibrations of footbridges through crowd flow control, *Struct. Control Health Monit*. 25 (2018) e2266, https://doi.org/10.1002/stc.2266.

[16] E. Shahabpoora, A. Pavic, V. Racic, Structural vibration serviceability: New design framework featuring human-structure interaction, *Eng. Struct*. 136 (2017) 295–311, https://doi.org/10.1016/j.engstruct.2017.01.030.

[17] W. Shi, L. Wang, Z. Lu, Study on self-adjustable tuned mass damper with variable mass, *Struct. Control Health Monit*. 25 (2018) e2114, https://doi.org/10.1002/stc.2114.

[18] S. Živanović, A. Pavic, P. Reynolds, Probability-based prediction of multi-mode vibration response to walking excitation, *Eng. Struct*. 29 (2007) 942–954, https://doi.org/10.1016/j.engstruct.2006.07.004.

[19] Y. Daniel, O. Lavan, R. Levy, Multiple-tuned mass dampers for multimodal control of pedestrian bridges, *J. Struct. Eng*. 138 (2012) 1173–1178, https://doi.org/10.1061/(ASCE)ST.1943-541X.0000527.

[20] E. Lai, C. Gentile, M.G. Mulas, Experimental and numerical serviceability assessment of a steel suspension footbridge, *J. Constr. Steel Res*. 132 (2017) 16–28, http://doi.org/10.1016/j.jcsr.2017.01.005.

[21] E. Caetano, Á. Cunha, C. Moutinho and F. Magalhães, Studies for controlling human-induced vibration of the Pedro e Inês footbridge, Portugal. Part 2: Implementation of tuned mass dampers, *Eng. Struct*. 32 (2010) 1082–1091. doi: 10.1016/j.engstruct.2009.12.033.

[22] F. J. Jiménez-Alonso and A. Sáez, Robust optimum design of tuned mass dampers to mitigate pedestrian-induced vibrations using multi-objective genetic algorithms, *Struct. Eng. International* 27(4) (2017) 492–501. doi: 10.2749/222137917X14881937844685.

[23] S. Qin, Y-L. Zhou and J. Kang, Footbridge serviceability analysis: from system identification to tuned mass damper implementation, *KSCE J. Civil Eng*. 23(2) (2019) 754–762. doi: 10.1007/s12205-018-0985-7.

[24] Q. Li, J. Fan, J. Nie, Q. Li and Y. Chen, Crowd-induced random vibration of footbridge and vibration control using multiple tuned mass dampers, *J. Sound Vib*. 329 (2010) 4068–4092. doi:10.1016/j.jsv.2010.04.013.

[25] D. Wang, C. Wu, Y. Zhang and S. Li, Study on vertical vibration control of long-span steel footbridge with tuned mass dampers under pedestrian excitation, *J. Constr. Steel Res*. 154 (2019) 84–98. doi: 10.1016/j.jcsr.2018.11.021.

[26] C. M. Casado, I. M. Díaz, J. de Sebastián, A. V. Poncela and A. Lorenzana, Implementation of passive and active vibration control on an in-service footbridge, *Struct. Control Health Monit*. 25 (2013) e2208. doi: 10.1002/stc.2208.

[27] C. Moutinho, Á. Cunha, E. Caetano and J. M. de Carvalho, Vibration control of a slender footbridge using passive and semiactive tuned mass dampers, *Struct. Control Health Monit*. 25 (2018) e2208. doi: 10.1002/stc.2208.

[28] J. Contreras-Lopez, F. Ornelas-Tellez and E. Espinosa-Juarez, Optimal control for footbridges' vibration reduction based on semiactive control through magnetorheological dampers, *Int. J. Struct. Stab. Dyn*. 19(9) (2019) 1950110.

[29] S. Zhou, Finite beam element considering shear-lag effect in box girder, *J. Eng. Mech*. 136 (2010) 1115–1122, https://doi.org/10.1061/(ASCE)EM.1943-7889.0000156.

[30] Z. Lin, J. Zhao, Modeling inelastic shear lag in steel box beams, *Eng. Struct*. 41 (2012) 90–97, http://dx.doi.org/10.1016/j.engstruct.2012.03.018.

[31] Z. Zhang, B. Li, Shear lag effect in tension flange of RC walls with flanged sections, *Eng. Struct*. 143 (2017) 64–76, https://doi.org/10.1016/j.engstruct.2017.04.017.

[32] G. Zhou, A. Li, J. Li, et al, Beam finite element including shear lag effect of extra-wide concrete box girders, *J. Bridge Eng*. 23 (2019) 04018083, https://doi.org/10.1061/(ASCE)BE.1943-5592.0001297.

[33] Z. Luo, H. Yuan, X. Niu, A new approach for free vibration analysis of thin-walled box girder considering shear lag effect, *Adv. Civ. Eng*. 2019 (2019) 1–10, https://doi.org/10.1155/2019/3902828.

[34] W. Zhou, et al., Vibration analysis of steel-concrete composite box beams considering shear lag and slip, *Math. Probl. Eng*. 2015 (2015) 601757, http://dx.doi.org/10.1155/2015/601757.

[35] L. Jiang, et al., Analysis of flexural natural vibrations of thin-walled box beams using higher order beam theory, *Struct. Design Tall Spec. Build*. 28 (2019) e1659, https://doi.org/10.1002/tal.1659.

[36] H. Cai, H. Lu, Z. Tang, Vibration properties research on curved box girder considering shear lag effects, *World Earthq. Eng*. 32 (2016) 239–244.

[37] Y. Zhang, P. Huang, Free vibration charateritiscs of simply supported box girder with effect of shear lag, *Journal of Architecture and Civil Engineering* 22 (2) (2005) 40–42.

[38] W. Zhou, L. Jiang, J. Qi, Analysis of free vibration characteristic of thin-wall box-girder considering shear lag and shear deformation, *Chinese Journal of Computational Mechanics* 30 (6) (2013) 802–806.

[39] Y. Zhang, L. Jiang, W. Zhou, Y. Feng, Shear Lag Effect and Accordion Effect on Dynamic Characteristics of Composite Box Girder Bridge with Corrugated Steel Webs. *Applied Sciences* 10(12) (2020) 4346.

[40] X. Wei, J. Russell, S. Živanović and J. Toby Mottram, Measured dynamic properties for FRP footbridges and their critical comparison against structures made of conventional construction materials, *Composite Structures* 223 (2019) 110956: 1-16. https://doi.org/10.1016/j.compstruct.2019.110956.

[41] H. Bachmann and W. Ammann, Vibrations in structures: induced by man and machines, *IABSE-AIPC-IVBH*, Zurich, Switzerland.

[42] E.C. Butz, Beitrag zur Berechnung fußgängerinduzierter Brückenschwingungen (PhD thesis), *RWTH Aachen*, 2006.

[43] Y. Matsumoto, S. Sato, T. Nishioka, et al, A study on dynamic design of pedestrian over-bridges, Trans. *JSCE* 205(1972) 83–90.

[44] P. Young, Improved floor vibration prediction methodologies, *ARUP Vibration Seminar*, October 4, 2001.

[45] R.L. Hughes, The flow of human crowds, *Annu. Rev. Fluid Mech*. 35 (2003) 169–182, https://doi.org/10.1146/annurev.fluid.35.101101.161136.

[46] Zhiqiang Zhang, et al. Simulation and Measurement of Human-Induced Vibrations of the Beijing Olympic Watchtower with Tuned Mass Dampers. *Journal of Performance of Constructed Facilities*. 2017, 31(6): 04017095. 10.1061/(ASCE)CF.1943-5509.0001089

[47] Ferreira, F and Simoes, L. Optimum Design of a Controlled Cable-Stayed Footbridge Subject to a Running Event Using Semiactive and Passive Mass Dampers. *Journal of Performance of Constructed Facilities*. 2019, 33(3). https://doi.org/10.1061/(ASCE)CF.1943-5509.0001285

[48] J.P. Den Hartog, Mechanical Vibrations, *Dover Publications, New York*, 1985.